J Herbmed Pharmacol. 2025; 14(4): 405-416.

http://www.herbmedpharmacol.com doi: 10.34172/jhp.2025.52810

Journal of Herbmed Pharmacology

# Impact of bio-computational tools for early detection of competent drug possibilities from *Zingiber officinale* Roscoe against adiponectin protein of type 2 diabetes mellitus and cardiovascular disease

**Chandra Sekhar Tripathy[1], Santosh Kumar Behera[2*], Sagarika Parida[1*]**

[1]Department of Botany, School of Applied Sciences, Centurion University of Technology and Management, Odisha, India
[2]Central Instrumentation Facility, National Institute of Pharmaceutical Education and Research, Ahmedabad, Gujarat, India

**ARTICLE INFO**

***Article Type:***
Original Article

***Article History:***
Received: 5 Nov. 2024
Revised: 5 Apr. 2025
Accepted: 13 Apr. 2025
epublished: 1 Oct. 2025

***Keywords:***
Galanolactone
Insulin resistance
Obesity
Diabetes mellitus
*Zingiber officinale*

**ABSTRACT**

**Introduction:** Dysbiosis of adiponectin is linked with an unhealthy gut microbiome resulting a decrease in the amount of adiponectin that induces type 2 diabetes mellitus (T2DM), obesity, dyslipidemia, thrombophilia, and cardiovascular disease (CVD). CVD, particularly stroke and heart attacks, is the prime reason for death among T2DM patients due to lower amounts of adiponectin, expressed by the gene ADIPOQ. Lower levels of adiponectin are strongly connected with insulin resistance and hyperinsulinemia. Research on the relationship between adiponectin and obesity, T2DM, and CVD is limited and the gaps need to be explored. Considering the importance of adiponectin, the current investigation was carried out through the screening of the phytocompounds from *Zingiber officinale* Roscoe against adiponectin to find out the potent phytocompounds for enhancing the production of adiponectin.

**Methods:** *In silico* investigation approaches such as Lipinski's rule of five, network analysis molecular docking, and molecular dynamics simulations were performed to explore the impact of adiponectin in T2DM and CVD comorbidities and its therapeutics.

**Results:** Fifteen out of 24 compounds satisfied Lipinski's rule of five that were further processed in various *in silico* studies along with the standard metformin. The docking studies revealed that the compound galanolactone with the highest binding affinity of -7.0 kcal/mol against Adiponectin was better than metformin.

**Conclusion:** The bio-computational tools explored an effective natural compound galanolactone identified with better efficacy than metformin in enhancing the levels of adiponectin that might ultimately be beneficial in the treatment of T2DM and CVD.

*Implication for health policy/practice/research/medical education:*
The study gives insight into the medicinal values of the rhizome of *Zingiber officinale* through this *in silico* approach for the treatment of type 2 diabetes and cardiovascular disease (CVD) from its potential compounds against adiponectin protein.

*Please cite this paper as:* Tripathy CS, Behera SK, Parida S. Impact of bio-computational tools for early detection of competent drug possibilities from *Zingiber officinale* Roscoe against adiponectin protein of type 2 diabetes mellitus and cardiovascular disease. J Herbmed Pharmacol. 2025;14(4):405-416. doi: 10.34172/jhp.2025.52810.

## Introduction

Type 2 diabetes mellitus (T2DM) is a prominent metabolic disorder, which elevates the probability of establishing diabetic cardiomyopathy and atherosclerotic cardiovascular disease (CVD). Heart failure can result from CVD through several mechanisms, which include myocardial infarction and persistent arterial overload. Although the majority of those influenced possess risk factors for both T2DM and CVD, including insulin resistance, obesity, dyslipidemia, thrombophilia, and inflammation, reports are scanty about the consequences of both conditions. CVD is one of the most prevalent

***Corresponding authors**: Sagarika Parida, Email: sagarika.parida@cutm.ac.in; Santosh Kumar Behera, Email: bioinfo.santosh@gmail.com

medical emergencies in the entirety of human health (1). Investigations provide evidence that the vulnerability of coronary artery disease and cardiac arrest is roughly two to four times higher in individuals with diabetes. In addition, it signifies that type 2 diabetes is a risk factor for causing heart disease and stroke (2). Due to low levels of adiponectin, CVD is the most prevalent cause of death among people suffering from type 2 diabetes and is strongly integrated with insulin resistance and hyperinsulinemia. The shift in the regulation of glucose and lipid metabolism by adiponectin demonstrates that adiponectin is an adipokine that is susceptible to insulin. By stimulating protein kinase B (Akt) activity across multiple insulin organs of concern, the adaptor protein containing pleckstrin homology domain (APPL1) promotes insulin action and secretion. Adiponectin is essential for averting CVD, especially whenever it comes to ailments like atherosclerosis, hypertension, and cardiopulmonary hypertrophy that are linked to aberrant lipid and glucose metabolism (3). The four different domains of adiponectin—an N-terminal signal peptide, a variable domain, a collagenous domain, and a C-terminal C1q-like globular domain—were discovered in the middle decades of the 1990s. Encompassing 244 amino acids (4), adiponectin originates on chromosome 3q27 (5), anatomically associated with T2DM and CVD (6).

Hypoadiponectinemia has been suspected in coronary artery disease, elevated carotid intima-media thickness, and endothelial dysfunction, as demonstrated by numerous clinical studies. Adiponectin's consequences at the vascular level include a decrease in the expression of E-selectin, vascular cell adhesion molecule-1, and intercellular adhesion molecule-1. Additionally, they prevent macrophages from turning into foam cells and smooth muscle cells from proliferating and migrating, both of which promote atherosclerosis. As a result, low blood adiponectin levels have been confirmed to be a risk factor for CVD; individuals with T2DM who have low levels of this protein are more likely to develop early arteriosclerosis. Individuals with T2DM are more susceptible to CVD due to lower blood adiponectin levels (7); a lower concentration of adiponectin induces heart stroke, myocardial infarction (8), and acute ischemic stroke (9). Despite the existing reports on the association of adiponectin with obesity, T2DM, and CVD, there are research gaps and paradox statements that are to be explored to understand the relationship among the comorbidities. Hence, to unzip the authenticity of the association between T2DM and CVD, and its potential therapeutics, an in-silico investigation was carried out by considering the targeted gene, adiponectin which has been reported to have a significant impact on causing T2DM through resisting insulin production and subsequently leading the risk factors for CVD, i.e., heart stroke (10). Furthermore, the current investigation focuses on exploring potential phytocompounds that could act as a key enhancer of insulin production by interacting with the targeted gene, adiponectin, which could be therapeutics for both T2DM and CVD, as there are hardly any specific drugs available in the market against the risk factor gene; this pertains to the development of new efficient drug candidates on an urgent basis.

In this study, natural compounds were taken as sources for predicting drug candidates. The plant taken for the survey was *Zingiber officinale* Roscoe (ginger). The rhizome part of the plant has many medicinal properties, and from thousands of years ago, it has been used in Ayurveda as a source of medicine to cure heart problems and treat stomach upset, diarrhea, and nausea. It decreases the joint pain caused by arthritis, and is valid in the treatment of heart and lung diseases, relieves cough, cold, and sore throat (11). *Z. officinale* has been reported in having anti-diabetic activities with *in vitro* and *in silico* validation studies. The chemical composition of the rhizome of the plant contains medicinal properties (12). Ginger is also reported as a hot remedy for the early treatment of CVD. Several human trials have also been made with better results on the effective use of ginger extract against CVD (13).

In the current investigation, a network and pharmacology-based bio-computational investigation approach was carried out for targeting the adiponectin protein. To the best of our knowledge, it is the first ever *in silico* investigation that attempted to find a single bio-molecular solution for therapeutics and safeguard the patient with T2DM and complications with CVD. The findings of this investigation will be significantly helpful for the development of drug candidates from natural sources, providing a resolution to decrease mortality and morbidity rates around the globe that may need further *in vitro* and *in vivo* validations.

## Materials and Methods

### Retrieval of protein information

Adiponectin protein sequence, structure, and function data were obtained from literature reviews and the UniProtKB database (https://www.uniprot.org/) (14), having UniProt ID: Q15848 (ADIPO_HUMAN). With PDB ID 6U66 and resolution 0.99 Å, the three-dimensional structure of adiponectin was obtained from the Protein Data Bank (PDB), a repository managed by the Research Collaboratory for Structural Bioinformatics (RCSB). This database provides access to experimentally determined molecular structures, enabling researchers to analyze and utilize structural data for scientific investigations (15). 136 (109-244) amino acids (aa) were identified to be contained in Chain A of adiponectin. The BIOVIA Discovery Studio 4.5 Visualizer (BIOVIA, San Diego, CA, USA) was employed to discard the additional chains and co-crystallized molecules.

### Repossession of phytoconstituents, and Lipinski's rule of five analyses

Literature review was conducted to find out the reported active phytochemicals from *Z. officinale*. The phytochemicals were retrieved from the published literature by searching databases like PubMed, Google Scholar, and other reputed journal sites. Compound IDs in Structure Data Format (SDF) were implemented to repossess the structural data of the compounds from the PubChem database (16). The BIOVIA Discovery Studio 4.5 Visualizer was incorporated to convert the structures to.pdb format. All the retrieved phytocompounds were screened through the TargetNet web server (17) for analysis of Lipinski's rule of five to select the orally active potential phytocompounds. The phytocompounds were processed through Lipinski's Rule of five (18), an essential prerequisite when selecting a medication.

### Network based protein-protein interaction study

The targeted protein adiponectin was subjected to network analysis to explore its interlinked genes and diseases associated with their expressions by using STRING (Search Tool for the Retrieval of Interacting Genes/Proteins) server (19) and WebGesalt (WEB-based GEne SeT AnaLysis Toolkit) server (20), respectively.

### Prediction of active sites and molecular docking simulation

The active site residues linked to the binding site dynamics of the adiponectin protein were predicted by integrating the consensus outcomes from multiple computational tools, including CASTp (21), DEPTH (accessible at http://cospi.iiserpune.ac.in/depth), and the Grid-based HECOMi finder (GHECOM) (available at https://pdbj.org/ghecom/) (22). These servers were employed to ensure a comprehensive and accurate identification of the functional regions within the protein structure. The molecular docking study was performed using the well-known docking tool i.e AutoDock vina to find the optimal binding natural compounds (23). The drug metformin was taken as standard because of its effectiveness for diabetic and CVDs. Metformin is mostly recommended by physicians around the world and has good market coverage (24). The spatial coordinates, including the x, y, and z axes, were determined and assigned utilizing AutoDock 4.2 software, based on the grid parameters derived from the protein structure. This approach ensured precise alignment and positioning for subsequent molecular docking analyses (25). For the convenience of comprehensive computational analysis, the best-docked complexes were initially characterized and then accompanied altogether by considering intermolecular hydrogen (H)-bonds, binding energy values, ligand potency, and other hydrophobic and electrostatic interactions. Leveraging BIOVIA Discovery Studio 4.5's 2D interaction module, the potential existence of intermolecular associations between protein–drug/compound complexes was assessed.

### Quantum computation

Based on predictions established through density functional theory (DFT), the study estimated the ligands' efficiency and vulnerability by executing a quantum computation simulation. To study the rate of reactivity of the molecules, a quantum computation study was achieved through Orca program 4.2 tool (26). Using quantum computation assessment, the lowest unoccupied molecular orbital (LUMO) and highest occupied molecular orbital (HOMO) energies were reported.

### Assessment of molecular dynamics (MD) simulation

Assessment of MD is an excellent computational tool for predicting and assessing the physical movements of atoms and molecules in the framework of macromolecular structure-to-function acquaintances (27). The dynamic "evolution" of the system is illustrated through the permitting of the atoms and molecules to interact for a predetermined amount of time (28). For verification of drug/compound binding modalities and providing an exhaustive representation of the protein-ligand complex, we accomplished dynamics simulations of the Apo (protein) and Holo (protein-ligand) implementing the Desmond program. An MD simulation enduring 100 ns was performed on the ligand-protein complexes that achieved the best score. The MD process entailed heating, equilibration, and minimization (29). Protein-ligand complexes have been reduced using the OPLS4 force field; atomic coordinates and topology were generated automatically (30). Subsequently, an orthorhombic box (15×15×10 Å) model of SPC solvent was adopted to soak up the chemical. 0.15 M NaCl was comprised to neutralize the pH. Implementing the Particle Mesh Ewald (PME) boundary circumstances, the water box was first activated to ensure that no solute atoms were located below 10 Å of the border. The NPT ensemble was implemented to simulate the complete system at 300 K for 100 ns. Root means square deviation (RMSD) and root mean square fluctuation (RMSF) envision were used to investigate the protein's modifications to structure and dynamic behavior. The variation between a protein's backbones from its originally formed structural conformation to its ultimate location was tracked by RMSD. A protein or complex's flexible region can be positioned employing the RMSF approach (31). The accomplished interaction diagram revealed the most plausible ligand binding process at the protein's binding site (32).

### Principal component analysis (PCA)

The statistical approach known as PCA facilitates the distinction between collective and local dynamics by partitioning enormous motional data sets into smaller

principal component subsets (33). The indispensable dynamics approach was applied to do the PCA. To achieve synchronized movements in the Apo and Holo states of the protein, Schrodinger Maestro v 2022.4's essential_dynamics.py software was implemented.

## Results

### Screening of phyto-constituents

The literature review could explore twenty-four number of compounds (34,35). The retrieved twenty-four compounds were aframodial, alpha-muurolene, beta-bisabolene, beta-cadinene, beta-santalol, beta-sesquiphellandrene, copaene, galanolactone, germacrene D, gingerenone A, gingerol, gingesulfonic acid, geraniol, isogingerenone B, nerolidol, sesquiphellandrene, shogasulfonic acid A, paradol, shogoal, zingiberol, zingerone, zingiberene, zingiberenol, and zonarene. Out of these compounds, only 15 compounds satisfied Lipinski's rule of five completely that were further analyzed by molecular docking analysis (Table 1).

### Development and evaluation of protein-protein interaction network

The protein-protein interaction network of adiponectin with its associated proteins was generated using the STRING database (https://string-db.org/) through the interactions with each other to explore the most significant genes throughout the network that became apparent. The STRING database research demonstrated the adiponectin interaction network, spanning ten distinct genes: CDH13, RETN, CFD, PLIN1, PPARG, LEP, PPARGC1A, ADIPOR1, ADIPOR2, and INS.

The protein-protein interaction graph of STRING database illustrated the association of adiponectin with most of the genes in the network. Further, all these associated genes were analyzed through the WebGesalt server to predict the relative chance of occurrence of diseases with the expression of associating diseases. These 11 interacting genes were subjected to the gene input box of the ORA sample run module of WebGesalt version 2019. The following parameters were selected: Homo sapiens under Organism of interest, Over-representation analysis under the Method of interest, and disease (Disgenet) under Functional database. Further, the submission was followed by the retrieval of consequence enrichment results. It was found that the genes associated with adiponectin could cause diseases like non-insulin-dependent diabetes mellitus, heart failure, diabetes mellitus, female infertility, and Barrett esophagus. From evidenced-based enrichment results it was found that the protein adiponectin was expressed in both diabetes mellitus and heart failure. This signified that a decrease in the amount of adiponectin was responsible for causing T2DM and CVD. Table 2 gives enrichment results of the genes responsible for diseases and Figure 1 depicts the genes linked with adiponectin protein and the graphic representation of a volcano plot of diseases associated with the genes.

### Annotation of binding sites and molecular docking analysis

The amino acids such as Leu119, Thr121, Val123, Ile125, Asn127, Met128, Pro129, Thr147, and Gln214 that are involved with the active site advancement of

**Table 1.** Phytocompounds from *Zingiber officinale* Roscoe with satisfied Lipinski rule of five

| Phytochemicals name | TPSA (<140 Å²) | MR (40-130 cm³/mol) | MW (≤500 g/mol) | HBD (≤5) | HBA1-(Hydrogen bond acceptors) (≤10) | LogP (≤5) |
|---|---|---|---|---|---|---|
| Aframodial | 46.67 | 92.441 | 318.4504 | 0.0 | 3.0 | 4.1024 |
| Beta-santalol | 20.23 | 69.9448 | 220.35046 | 1.0 | 1.0 | 3.6976 |
| Galanolactone | 38.83 | 91.212 | 318.4504 | 0.0 | 3.0 | 4.2614 |
| Gingerenone A | 75.99 | 101.493 | 356.41226 | 2.0 | 5.0 | 3.8057 |
| Gingerol | 66.76 | 84.5478 | 294.38594 | 2.0 | 4.0 | 3.2338 |
| Gingesulfonic acid | 109.28 | 93.9218 | 358.44974 | 2.0 | 6.0 | 4.2101 |
| Geraniol | 20.23 | 50.3978 | 154.24932 | 1.0 | 1.0 | 2.6714 |
| Isogingerenone B | 85.22 | 107.985 | 386.43824 | 2.0 | 6.0 | 3.8143 |
| Nerolidol | 20.23 | 73.9968 | 222.36634 | 1.0 | 1.0 | 4.3963 |
| Shogasulfonic acid A | 138.74 | 112.5028 | 438.49134 | 3.0 | 8.0 | 3.9768 |
| Paradol | 46.53 | 83.386 | 278.38654 | 1.0 | 3.0 | 4.263 |
| Shogoal (Si) | 46.53 | 82.912 | 276.37066 | 1.0 | 3.0 | 4.039 |
| Zingiberol | 20.23 | 70.4568 | 222.36634 | 1.0 | 1.0 | 3.92 |
| Zingerone | 46.53 | 54.544 | 194.22706 | 1.0 | 3.0 | 1.9224 |
| Zingiberenol | 20.23 | 72.3568 | 222.36634 | 1.0 | 1.0 | 4.0861 |

TPSA: Topological polar surface area; MR: Molar refractivity; MW: Molecular weight; HBD: Hydrogen bond donors; HBA : Hydrogen bond acceptors; LogP: Logarithm of the partition coefficient (P).

**Table 2.** Gene interaction-based functional enrichment analysis of disease associations

| Gene set | Description | Interacting genes | *P* value | FDR |
|---|---|---|---|---|
| C0011860 | Diabetes mellitus, non-insulin-dependent | ADIPOQ, INS, LEP, PPARG, PPARGC1A, RETN | 1.8814e-8 | 0.000028588 |
| C0018801 | Heart failure | ADIPOQ, CFD, INS, PPARG, PPARGC1A, RETN | 3.1424e-8 | 0.000028588 |
| C0011849 | Diabetes mellitus | ADIPOQ, INS, PLIN1, PPARG | 0.0000038481 | 0.0020004 |
| C0021361 | Female infertility | ADIPOR1, ADIPOR2, LEP | 0.0000079602 | 0.0032186 |
| C0004763 | Barrett esophagus | CDH13, PPARG | 0.00019604 | 0.035670 |

FDR: False discovery rate.

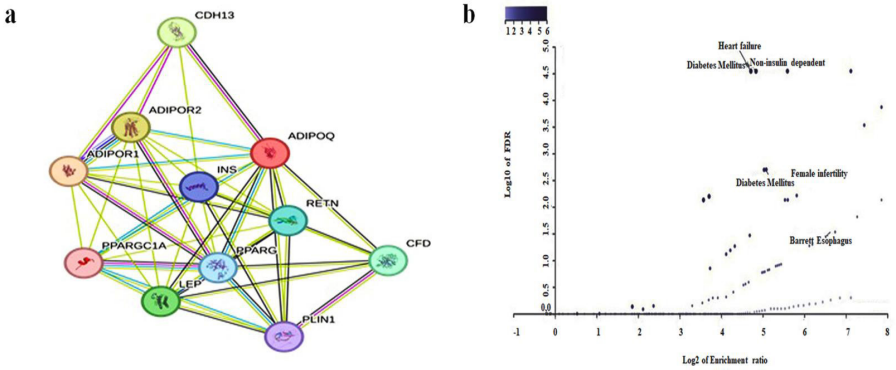


**Figure 1. Protein-protein interaction network of genes and Volcano plot of disease model associations.** (a) ADIPOQ's network of interaction between proteins retrieved from the STRING database. The network of predicted interactions with other proteins is rounded up by the expected network. The nodes in the network are proteins and the edges are likely associations between the proteins. Regional evidence is symbolized in green, co-occurrence evidence in blue, experimental evidence in purple, database evidence in light blue, text mining in light green, and co-expression information in black. The colored lines on the edges imply the existence of different types of evidence used for identifying potential associations. Additionally, the interaction's degree of anticipation confidence is represented by the edge thickness (b) Description of the closely associated diseases through Volcano plot. Representation of disease associated with the low amount of adiponectin (ADIPOQ) with heart failure and diabetes mellitus found to be closely connected to each other.

the adiponectin protein are indicated in the consensus results from each web server. Grid analysis was executed employing the AutoDock program, an acclaimed docking software system that is significantly utilized for evaluating compounds against potential targets. The protein was provided with Kollman charges using ADT v.1.5. The adiponectin grid included each of the following assessments, gaps, and qualities that permitted the molecule or drug to fully broaden the framework; grid dimension values were X-46, Y-58, and Z-64, followed by x-centering: -20.56, y-centering: 130.753, and z-centering: -9.636.

Fifteen compounds following Lipinski's rule of five were docked against the protein at its determined grid box values using the AutoDock vina tool. The molecular docking revealed the compound galanolactone with the highest binding energy of -7.0 kcal/mol against adiponectin protein forming 3 Hydrogen bonds with Thr124 and Asn222 amino acid residues, respectively, followed by other compounds. The marketed compound metformin revealed a binding energy of -4.5 kcal/mol, less than the natural compound galanolactone. The molecular docking results of all 15 phytocompounds and metformin (marketed) are represented in Table 3. Figure 2 depicts the protein-ligand interaction of the adiponectin-galanolactone complex in 3D and 2D format.

To properly understand and authenticate the binding processes that regulate protein-ligand interaction over an identifiable period, the docked complex was subsequently put through MD simulations. adiponectin-galanolactone complex intermolecular connections were demonstrated by deploying BIOVIA Discovery Studio 4.5 Visualizer.

## Quantum chemistry approaches using DFT

The relative reactiveness of the natural compound galanolactone was studied and compared with metformin (marketed), using the DFT of Orca program. The compound galanolactone showed a band gap energy of 12.574 eV. In contrast, metformin showed a band gap energy of 13.497 eV. Galanolactone displayed higher reactivity when analogized to metformin and entrenched its lowest band energy gap, implying that galanolactone is more reactive than metformin and may work faster inside the body. Table 4 represents the quantum simulation results for galanolactone and metformin at different energy values. Figure 3 is the visual representation of the calculated DFT results of galanolactone & metformin.

## MD simulation trajectory analysis

The highly intricate MD algorithm investigated how atoms and molecules came into contact within a system of physical connections between macromolecular

**Table 3.** Molecular docking scores of 15 phytoconstituents from *Zingiber officinale* Roscoe and metformin (marketed) docked against ADIPOQ protein

| Target protein | Compound/Drug | Binding energy (kcal/mol) | No. of H-bonds | H-bond forming residues | Average distance of H-bonds (Å) |
|---|---|---|---|---|---|
| Adiponectin (ADIPOQ) | Aframodial | -6.1 | 1 | His241 | 2.12036 |
| | Beta-santalol | -6.0 | 1 | Ser113 | 2.66036 |
| | Galanolactone | -7.0 | 3 | Thr124, Asn222 | 2.38278 |
| | Gingerenone A | -5.9 | 2 | Ser113, Leu238 | 2.306275 |
| | Gingerol | -5.6 | 1 | Ser113, Tyr137 | 2.326385 |
| | Gingesulfonic acid | -5.5 | 1 | Tyr111 | 2.25329 |
| | Geraniol | -4.8 | 2 | Ser113, Leu238 | 2.24603 |
| | Isogingerenone B | -5.5 | 1 | Tyr111 | 2.44912 |
| | Nerolidol | -5.6 | 1 | Tyr111 | 2.9014 |
| | Shogasulfonic acid A | -6.2 | 1 | Tyr111 | 2.2388 |
| | Paradol | -5.2 | 2 | Tyr137, Gln140 | 2.459395 |
| | Shogoal (Si) | -5.7 | - | - | - |
| | Zingiberol | -6.1 | 2 | Asp170, Ty189 | 2.466545 |
| | Zingerone | -5.3 | 1 | Asp170 | 2.56678 |
| | Zingiberenol | -5.9 | 1 | Ser113 | 2.32321 |
| | Metformin (marketed) | -4.5 | 6 | Arg131, Thr121, Val123, Pro129, Ile130 | 2.403488333 |

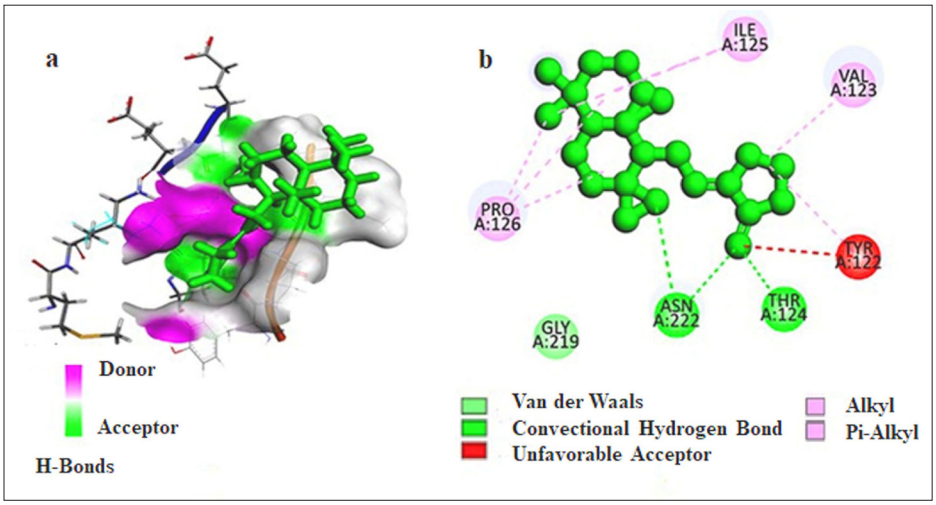


**Figure 2.** Drug-target interactions of adiponectin-galanolactone complex. (a) 3-dimensional (b) 2-dimentional.

components and their functions. The multifaceted evolution of the system was apparent in the intervals at which the atoms and molecules were enabled to interact. Long-term reliability of the docked complex was monitored using a 100 ns MD simulation incorporating structural variations in molecules and receptors.

Using the Desmond suit, the stability and attractiveness of the Apo and Holo systems (Apo: adiponectin; Holo1: adiponectin-galanolactone complex, Holo2: adiponectin-metformin complex) were assessed in order to determine the dynamic behavior and bonding mechanism. The RMSD pattern of the backbone atoms at 100 ns was used in assessing the dynamic firmness of the Apo and Holo systems for the adiponectin protein (Figures 4a and 4b).

In case of Holo1 state: Adiponectin-galanolactone complex showed a stable trajectory during ~25 to ~55 ns and ~75 to 85 ns of time period with RMSD values ranging from ~0.8 to ~0.40 Å and ~0.70 to 1.10 Å. Compared to its

**Table 4.** Electronic energy, energy in an atomic unit of highest occupied molecular orbital (HOMO), lowest unoccupied molecular orbital (LUMO), gap energy, and dipole moment of galanolactone and reported drug metformin

| Phytochemical name | Electronic energy(eV) | LUMO (eV) | HOMO (eV) | GAP energy (eV) | Dipole moment (Debye) |
|---|---|---|---|---|---|
| Galanolactone | -85197.88859 | 2.763 | -9.811 | 12.574 | 4.99527 |
| Metformin | -17810.66493 | 4.681 | -8.816 | 13.497 | 1.74138 |

eV: electron volt.

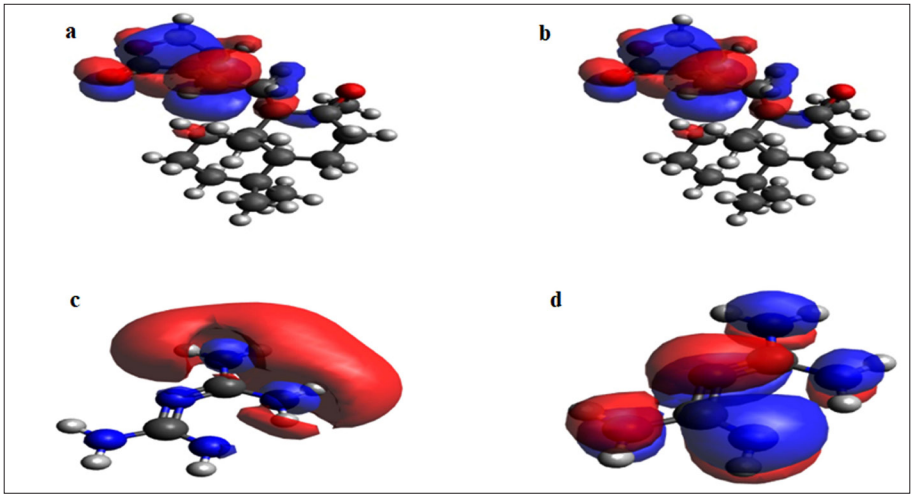


**Figure 3.** The lowest unoccupied molecular orbital (LUMO) and the highest occupied molecular orbital (HOMO) Plots of galanolactone (a and b) and metformin (c and d). These HOMO and LUMO diagrams exhibited diminished band gap energy and boosted reactivity. The positive electron density is indicated by red colour while blue colour indicates negative electron density.

Apo state, the values of Holo1 state are quite smaller, which defines a stable configuration. Adiponectin-metformin complex showed consistent deviations throughout the simulation cycle compared to its Apo state, which depicts its instability.

The backbone atoms of RMSD profile at 100 ns is presented in Figures 4a and 4b, illustrating the dynamic stability of both the Apo and Holo systems for ligands establishing complexes with the adiponectin protein. When evaluating the RMSD values of the two Holo states in the case of adiponectin, Holo1 demonstrated an uninterrupted trajectory and only minor variations from Holo2. This depicts that the compound galanolactone could bind more firmly with adiponectin and aid in maintaining rigidity by tailoring its molecular framework compared to metformin.

Further validation for the RMSD result emerged from RMSF, which quantified residue variability. The dispersion among various residues has been monitored in each state implementing RMSF plots. Thus, comparable to the Holo states, the Apo state observed more extensive fluctuations for adiponectin protein, demonstrating the simulation's constrained motions. For Holo1, the amino acid residues between 0 to 8, 25 to 30, 50 to 55, and 110 to 115 displayed significant variations within their Cα atoms contrary to alternate locations. For Holo2, a constant variation was observed between 10 to 30 and 78 to 88. Protein residues that communicate with the ligand are represented by green vertical bars. The results obtained endorse that residues in the Holo state may become more stationary compared to the ones in the Apo state due to ligand participation. Figures 4c and 4d depict the RMSF results.

During the 100 ns simulation, traits, especially the radius of gyration (rGyr), explicated compounds' resilience and overall compactness in the adiponectin protein's binding pocket. A ligand's rGyr can be used to identify how "extended" it is or how competent it is in forming a compactness with the target. The rGyr fluctuation graphs versus the simulation timeframe for adiponectin confirm that rGyr persists constantly across the simulation operation between ~25 to 55 ns, and again between ~85 ns to ~95 for Holo1, which revealed rGyr values ~3.78 to ~4.02 Å and ~3.88 to 4.01. Holo2 reflected rGyr values constant between ~85 to 85 ns simulation frame with values ~2.14 to ~2.23Å. The rGyr value of Holo1 was found to have more stable values than Holo2, defining its more rigidity, and Holo1 indicated that the galanolactone could potentially interact more with adiponectin. These outcomes of rGyr are potentially supported by RMSF analysis. Figures 4e and 4f depicts the rGyr results.

Amino acids have been emphasized by hydrophobic interactions between the solvent and key protein residues; the effectiveness of these interactions varies according to the solvent-accessible surface area (SASA). Under the SASA study, the binding of compounds may shift hydrophilic and hydrophobic interface zones, which might have a consequence on protein surface orientations in light of the shift in amino acid residues during the simulation of adiponectin spanning 70 to 100 ns. The Holo1 state portrayed SASA. In the specific instance of Holo1, the SASA appraisal was ~190Å2 to ~230Å2 during the amino acid residue shift simulation period between 20 ns to 60 ns. SASA values for Holo2 ranged between ~80Å2 to ~250Å2 during the simulation period between 5 to 18 ns, 38 to 45 ns, 60 to 70 ns, and 75 to 90 ns with constant deviations. This indicates that the shift in the symmetry of the protein's exterior could originate from amino acid residues of Holo states migrating from what is viewable to the concealed region, and Holo1 has less deviated SASA value, defining its more stability than Holo2. Figures 4g and 4h confirmed the solvent surface in the Holo processes.

## Hydrogen bond dynamics and stability analysis

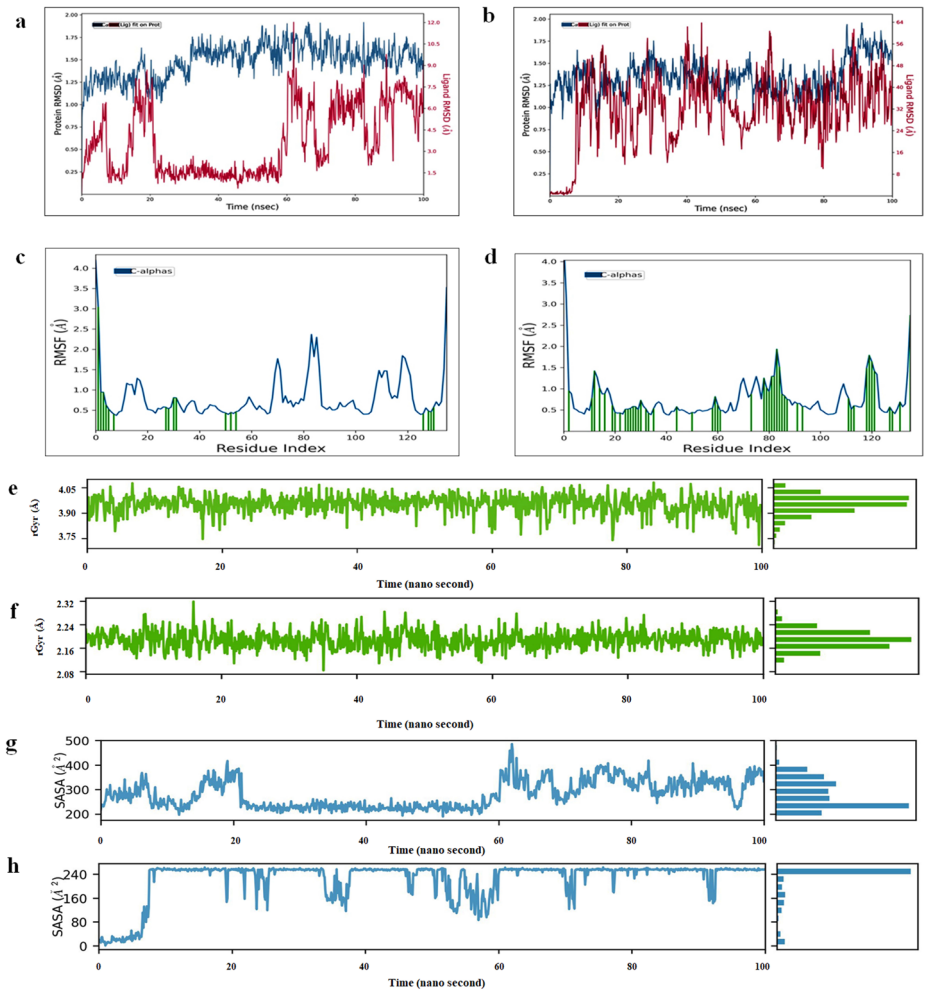


**Figure 4.** Morphological equilibrium within adiponectin's Apo and Holo states throughout 100 ns molecular dynamics simulations (MDS). (a) Backbone-root mean square deviation (RMSD) period of adiponectin-galanolactone complex and (b) Backbone RMSD of adiponectin-metformin complex. Conformational stability for Cα-Root mean square fluctuation (RMSF) profile of (c) Cα- RMSF of adiponectin-galanolactone complex (d) Cα-RMSF of adiponectin-metformin complex. Radius of gyration (rGyr) profile of (e) rGyr of adiponectin-galanolactone complex (f) rGyr of adiponectin-metformin complex. Solvent accessible surface area (SASA) analysis of (g) SASA of adiponectin-galanolactone complex (h) SASA of adiponectin-metformin complex.

Schrödinger release 2022-4 was implemented to plot the intermolecular hydrogen bonds of the Holo state across MD simulations, as illustrated in Figures 5a and 5b. The Holo states' simulation by computer illustrated variables associated with intermolecular hydrogen bonding. The coherence of the drug-target complex matched the aggregate number of H-bonds precisely throughout the entirety of the period of simulation. In Figure 5a, the Holo1 state simulation exhibited a steady supply of intermolecular hydrogen bonds. In the scenario of post-MD of Holo1, one H-bond forming residue (Ser113) is illustrated in Figure 5c. The reliability of the drug-target complex correlated precisely with the quantity of H-bonds across the simulation. H-bond-forming residues like Thr124 and Asn222 were broken during MD simulations of Holo1, and they have been substituted by new H-bond-forming residues (Ser113), van der Waals, and hydrophobic interactions. As perceived in Figure 5b, the simulation of the Holo2 state illustrated a fluctuating number of intermolecular hydrogen bonds throughout the experiment. In Figure 5d, the post-MD of Holo1 and Holo2 is portrayed by six H-bond-forming residues (Ile125, Arg131, Thr121, and Pro129). During MD simulations of Holo1, H-bond-forming residues such as Val123 and Ile130 were eliminated and their spots were replaced with new H-bond-forming residues (Ile125), van der Waals, and hydrophobic interactions. In spite of few novel interactions, the H-bond forming residue (Arg131, Thr121, Pro129) did not compensate. Figure 5e and 5f provides the three-dimensional structure of galanolactone and metformin.

## The assessment of principal components

The trace variations in the matrix of covariant values of backbone atoms across multiple states simulation regulations were assessed to gauge the flexibility of the Apo and Holo states. The trajectory projections from PC1 and PC2 captured the motion of the states in phase

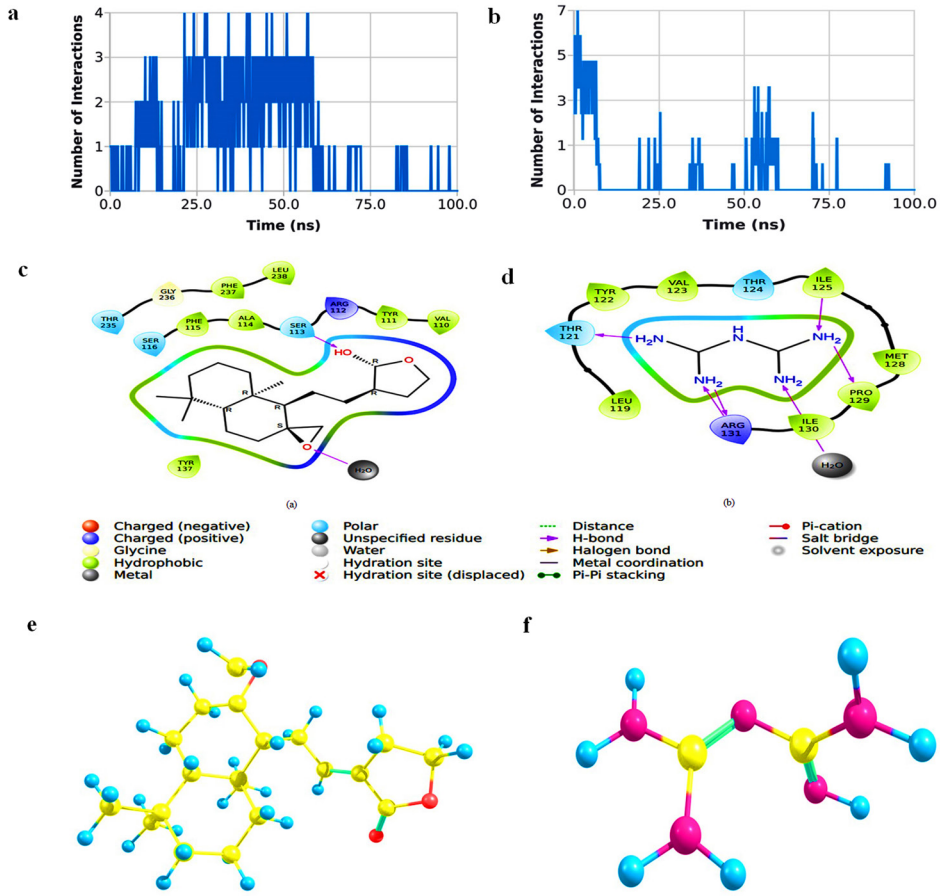


**Figure 5. Hydrogen-bond interaction pattern in drug-target complex during 100 ns simulation of simulation time period.** (a) H-bonds intensity of adiponectin-galanolactone complex. (b) H-bonds intensity of adiponectin-metformin complex. Two-dimensional (2-D) interaction of Post-Molecular Dynamics simulation ligand-target interaction analysis depicting intermolecular hydrogen bonding, electrostatic and hydrophobic contacts between (c) 2-D interaction of adiponectin-galanolactone complex (d) 2-D interaction of adiponectin-metformin complex. Three-dimensional structure of (e) galanolactone (f) metformin. Visualized using Chemcraft tool.

space. The relative motion of the Apo and Holo states in the wild-type and mutant protein-ligand complexes was seen by estimating the trajectories onto the first two principal components (PC1 and PC2), portrayed in Figure 6a and 6b. The scattering cloud of PCA plots illustrates that the Holo2: Adiponectin–metformin complex is more adaptable than the Holo1: Adiponectin–galanolactone complex. The versatility may be attributable to the motion and re-motion of atom configurations across the dual time course of the 100 ns time period simulation frame. All residues in the "adiponectin" protein have been identified to have both negatively (represented by blue colors) and positively (represented by red shades) pertinent motions, corresponding to the "Cross-correlation matrix" of the Cα- displacement (Figure 6c and 6d) that promotes the protein's random movement. Higher, dense, and disseminated favorably related motions emerged for Holo1, while higher negatively associated motions for adiponectin were revealed for Holo2.

The directional attributes of molecular motion have been illustrated by the vectorial representation of its elements. Projection vectors predominantly captured both internal and external dynamics, revealing the principal modes of movement. Upon graphical analysis, distinct porcupine plots (Figure 6e and 6f) exhibited pronounced curvature, indicative of complex motion patterns. These plots illustrated inward and outward projections, reflecting variations in flexibility and conformational dynamics. Such behavior likely arises from the continuous rearrangement of atomic configurations over the dual 100 ns simulation trajectory, highlighting the dynamic nature of the system.

## Discussion

The existing reports state that people in the adult stage with T2DM have an elevated risk of causing heart-related diseases, which implies heatstroke. In day-to-day life, it has become very common to see certain consequences of premature deaths. In T2DM, the body decreases the production of insulin, which results in the dysbiosis of glucose level in the body. The research depicts that, when there is an increase of glucose in the body, it damages

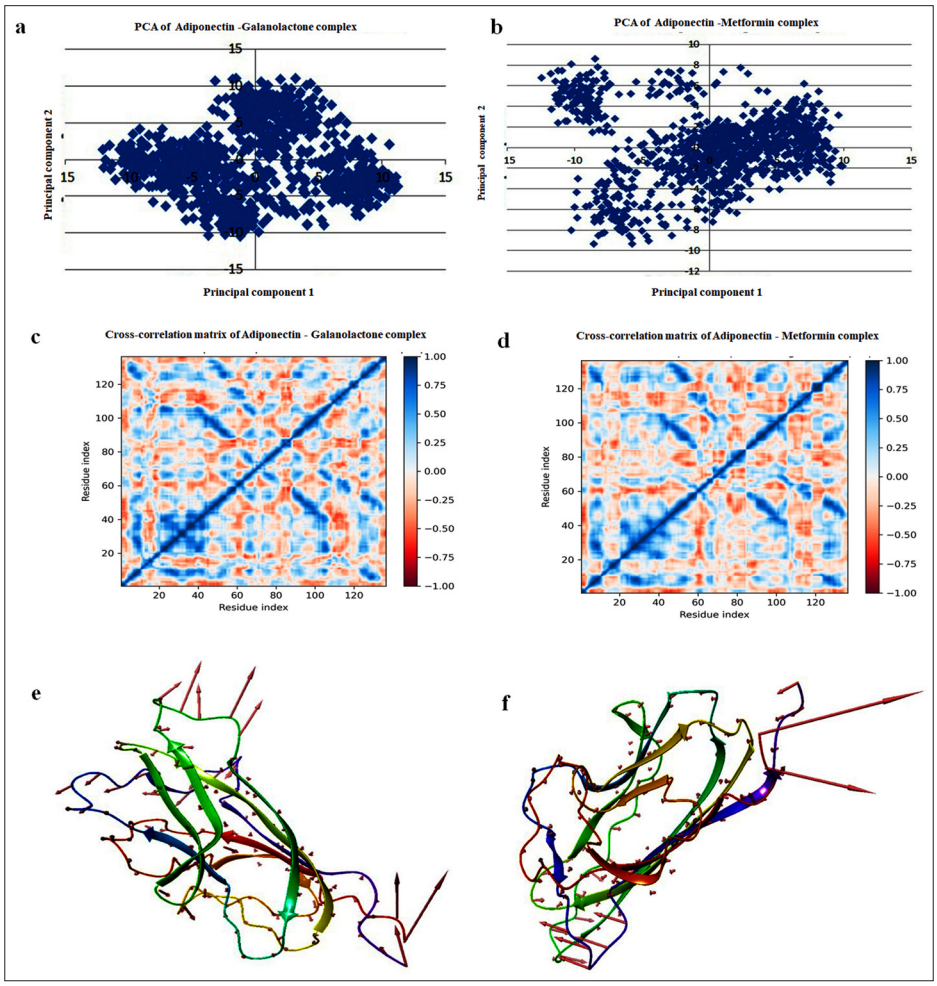


**Figure 6. Principal component analysis (PCA) visualization of the adiponectin protein complexes.** (a) PCA graph of adiponectin-galanolactone complex. (b) PCA graph of adiponectin-metformin complex. Graphic representation of cross-correlation matrices of adiponectin protein. (c) Cross-correlation matrix of adiponectin-galanolactone complex. (d) Cross-correlation matrix of adiponectin-metformin complex. Three-dimensional representation Porcupine plots after simulation. (e) Porcupine plot of adiponectin-galanolactone complex. (f) Porcupine plot of adiponectin-metformin complex.

the blood vessels of the heart, which develops fatty depositions known as atherosclerosis. In this case, the arteries get stiff enough developing plaque buildup in the walls leading to blockage for blood flow. The insufficient flow of blood in arteries leads to heart attacks, which is a serious condition leading to increase in mortality rate (37). In the overall scenario, the presence of the gene-specific workflow has also been observed around the world, which means there must be a common factor that is linked to the occurrence of both the diseases. Hence, the gene or the genetic factor responsible for the mortality and morbidity must be identified and targeted for its therapeutics. In this investigation, the protein adiponectin was targeted as it was reported to be associated with both T2DM and CVD, significantly (38). Numerous animal models of T2DM have been emerged using a combination of high-fat diet and low-dose streptozotocin administration. However, the specific mechanisms underlying cardiac dysfunction in these models, as well as the precise role of adiponectin in modulating such pathological changes, remain incompletely elucidated and require further comprehensive characterization (39). Therefore, keeping in concern, the paradox reports and insufficient authentication of interlinked co-morbidities of T2DM and CVD, the present *in silico* approach was perused, which could predict the vital role of gene ADIPOQ in the interlinked co-morbidities that could be managed with a single hindrance. The WebGesalt server, depicted the action of genes interacting with adiponectin, interlinked to cause T2DM and CVD more adversely. This states that the adiponectin protein is associated with T2DM and CVD with a decrease in the production of insulin that causes fat deposition in the artery of the heart preventing proper flow of oxygenated blood and blockage due to fat deposition leading to heart stroke. Therefore, the current study may be able to unravel galanolactone, a phytocompound from *Z. officinale*, popularly referred to as ginger, which may increase the synthesis of adiponectin in comparison to metformin. The MD simulation revealed its stability for its significantly anchored configuration

and trajectories. The compound galanolactone has also been reported as an anti-adipogenesis medicine (40). The term anti-adipogenesis proves that the compound is capable enough to inhibit the production of fat inside the body, which will enhance the capability of adiponectin protein by binding with it for the production of insulin and reducing the fat amount in the artery of the heart. These actions of the molecule clearly state to manage T2DM and CVD. The findings of this investigation could be preliminary that needs further *in vitro* and *in vivo* investigations, and intervention pharmaceutical industries to develop and commercialize the potential compound for the therapeutic management of diabetes and CVD.

## Conclusion

The current *in silico* investigation could explore the key gene ADIPOQ, which is associated with both the co-morbidities T2DM and CVD. Subsequently, it stated the potentiality of galanolactone, one of the natural compounds from *Z. officinale* as drug candidates for the therapy of T2DM and CVDs through the reduction of the blood sugar level and increase in insulin sensitivity.

## Authors' contribution

**Conceptualization:** Sagarika Parida.
**Data curation:** Santosh Kumar Behera.
**Formal analysis:** Chandra Sekhar Tripathy.
**Funding acquisition:** Chandra Sekhar Tripathy, Santosh Kumar Behera and Sagarika Parida.
**Investigation:** Sagarika Parida and Santosh Kumar Behera.
**Methodology:** Sagarika Parida, Chandra Sekhar Tripathy and Santosh Kumar Behera.
**Project administration:** Santosh Kumar Behera and Sagarika Parida.
**Resources:** Chandra Sekhar Tripathy and Santosh Kumar Behera.
**Software:** Chandra Sekhar Tripathy and Santosh Kumar Behera.
**Supervision:** Sagarika Parida and Santosh Kumar Behera.
**Validation:** Santosh Kumar Behera and Chandra Sekhar Tripathy.
**Visualization:** Chandra Sekhar Tripathy and Santosh Kumar Behera.
**Writing–original draft:** Chandra Sekhar Tripathy, Santosh Kumar Behera and Sagarika Parida.
**Writing–review & editing:** Santosh Kumar Behera and Sagarika Parida.

## Conflict of interests

The authors declare no conflict of interest.

## Data availability statement

Upon a reasonable request, data supporting these findings can be made available by the corresponding author.

## Ethical considerations

Authors declare no ethical issues.

## Funding/Support

Non-funded nor donor driven. Authors self-contributed equally for the work.

## References

1. Benjamin EJ, Blaha MJ, Chiuve SE, Cushman M, Das SR, Deo R, et al. Heart disease and stroke statistics-2017 update: a report from the American Heart Association. Circulation. 2017;135(10):e146-603. doi: 10.1161/cir.0000000000000485.
2. Martín-Timón I, Sevillano-Collantes C, Segura-Galindo A, Del Cañizo-Gómez FJ. Type 2 diabetes and cardiovascular disease: have all risk factors the same strength? World J Diabetes. 2014;5(4):444-70. doi: 10.4239/wjd.v5.i4.444.
3. Han W, Yang S, Xiao H, Wang M, Ye J, Cao L, et al. Role of adiponectin in cardiovascular diseases related to glucose and lipid metabolism disorders. Int J Mol Sci. 2022;23(24):15626. doi: 10.3390/ijms232415627.
4. Scherer PE, Williams S, Fogliano M, Baldini G, Lodish HF. A novel serum protein similar to C1q, produced exclusively in adipocytes. J Biol Chem. 1995;270(45):26746-9. doi: 10.1074/jbc.270.45.26746.
5. Das K, Lin Y, Widen E, Zhang Y, Scherer PE. Chromosomal localization, expression pattern, and promoter analysis of the mouse gene encoding adipocyte-specific secretory protein Acrp30. Biochem Biophys Res Commun. 2001;280(4):1120-9. doi: 10.1006/bbrc.2001.4217.
6. Vionnet N, Hani EH, Dupont S, Gallina S, Francke S, Dotte S, et al. Genomewide search for type 2 diabetes-susceptibility genes in French whites: evidence for a novel susceptibility locus for early-onset diabetes on chromosome 3q27-qter and independent replication of a type 2-diabetes locus on chromosome 1q21-q24. Am J Hum Genet. 2000;67(6):1470-80. doi: 10.1086/316887.
7. Liang W, Ye DD. The potential of adipokines as biomarkers and therapeutic agents for vascular complications in type 2 diabetes mellitus. Cytokine Growth Factor Rev. 2019;48:32-9. doi: 10.1016/j.cytogfr.2019.06.002.
8. Drechsler C, Krane V, Winkler K, Dekker FW, Wanner C. Changes in adiponectin and the risk of sudden death, stroke, myocardial infarction, and mortality in hemodialysis patients. Kidney Int. 2009;76(5):567-75. doi: 10.1038/ki.2009.200.
9. Tu WJ, Qiu HC, Liu YK, Liu Q, Zeng X, Zhao J. Elevated levels of adiponectin associated with major adverse cardiovascular and cerebrovascular events and mortality risk in ischemic stroke. Cardiovasc Diabetol. 2020;19(1):125. doi: 10.1186/s12933-020-01096-3.
10. De Rosa S, Arcidiacono B, Chiefari E, Brunetti A, Indolfi C, Foti DP. Type 2 diabetes mellitus and cardiovascular disease: genetic and epigenetic links. Front Endocrinol (Lausanne). 2018;9:2. doi: 10.3389/fendo.2018.00002.
11. Kumar Gupta S, Sharma A. Medicinal properties of *Zingiber officinale* Roscoe-a review. IOSR J Pharm Biol Sci. 2014;9(5):124-9. doi: 10.9790/3008-0955124129.
12. Zhu J, Chen H, Song Z, Wang X, Sun Z. Effects of ginger (*Zingiber officinale* Roscoe) on type 2 diabetes mellitus and components of the metabolic syndrome: a systematic review and meta-analysis of randomized controlled trials.

Evid Based Complement Alternat Med. 2018;2018:5692962. doi: 10.1155/2018/5692962.
13. Nicoll R, Henein MY. Ginger (*Zingiber officinale* Roscoe): a hot remedy for cardiovascular disease? Int J Cardiol. 2009;131(3):408-9. doi: 10.1016/j.ijcard.2007.07.107.
14. UniProt: a hub for protein information. Nucleic Acids Res. 2015;43(D1):D204-12. doi: 10.1093/nar/gku989.
15. Burley SK, Berman HM, Kleywegt GJ, Markley JL, Nakamura H, Velankar S. Protein Data Bank (PDB): the single global macromolecular structure archive. Methods Mol Biol. 2017;1607:627-41. doi: 10.1007/978-1-4939-7000-1_26.
16. Kim S, Chen J, Cheng T, Gindulyte A, He J, He S, et al. PubChem 2023 update. Nucleic Acids Res. 2023;51(D1):D1373-80. doi: 10.1093/nar/gkac956.
17. Yao ZJ, Dong J, Che YJ, Zhu MF, Wen M, Wang NN, et al. TargetNet: a web service for predicting potential drug–target interaction profiling via multi-target SAR models. J Comput Aided Mol Des. 2016;30(5):413-24. doi: 10.1007/s10822-016-9915-2.
18. Chen X, Li H, Tian L, Li Q, Luo J, Zhang Y. Analysis of the physicochemical properties of acaricides based on Lipinski's rule of five. J Comput Biol. 2020;27(9):1397-406. doi: 10.1089/cmb.2019.0323.
19. von Mering C, Huynen M, Jaeggi D, Schmidt S, Bork P, Snel B. STRING: a database of predicted functional associations between proteins. Nucleic Acids Res. 2003;31(1):258-61. doi: 10.1093/nar/gkg034.
20. Liao Y, Wang J, Jaehnig EJ, Shi Z, Zhang B. WebGestalt 2019: gene set analysis toolkit with revamped UIs and APIs. Nucleic Acids Res. 2019;47(W1):W199-205. doi: 10.1093/nar/gkz401.
21. Tian W, Chen C, Lei X, Zhao J, Liang J. CASTp 3.0: computed atlas of surface topography of proteins. Nucleic Acids Res. 2018;46(W1):W363-7. doi: 10.1093/nar/gky473.
22. Kawabata T. Detection of multiscale pockets on protein surfaces using mathematical morphology. Proteins. 2010;78(5):1195-211. doi: 10.1002/prot.22639.
23. Trott O, Olson AJ. AutoDock Vina: improving the speed and accuracy of docking with a new scoring function, efficient optimization, and multithreading. J Comput Chem. 2010;31(2):455-61. doi: 10.1002/jcc.21334.
24. Azimova K, San Juan Z, Mukherjee D. Cardiovascular safety profile of currently available diabetic drugs. Ochsner J. 2014;14(4):616-32.
25. Morris GM, Huey R, Lindstrom W, Sanner MF, Belew RK, Goodsell DS, et al. AutoDock4 and AutoDockTools4: Automated docking with selective receptor flexibility. J Comput Chem. 2009;30(16):2785-91. doi: 10.1002/jcc.21256.
26. Neese F. The ORCA program system. Wiley Interdiscip Rev Comput Mol Sci. 2012;2(1):73-8. doi: 10.1002/wcms.81.
27. Behera SK, Vhora N, Contractor D, Shard A, Kumar D, Kalia K, et al. Computational drug repurposing study elucidating simultaneous inhibition of entry and replication of novel corona virus by Grazoprevir. Sci Rep. 2021;11(1):7307. doi: 10.1038/s41598-021-86712-2.
28. Durrant JD, McCammon JA. Molecular dynamics simulations and drug discovery. BMC Biol. 2011;9:71. doi: 10.1186/1741-7007-9-71.
29. Raghu R, Devaraji V, Leena K, Riyaz SD, Rani PB, Kumar BS, et al. Virtual screening and discovery of novel aurora kinase inhibitors. Curr Top Med Chem. 2014;14(17):2006-19. doi: 10.2174/1568026614666140929151140.
30. Shivakumar D, Williams J, Wu Y, Damm W, Shelley J, Sherman W. Prediction of absolute solvation free energies using molecular dynamics free energy perturbation and the OPLS force field. J Chem Theory Comput. 2010;6(5):1509-19. doi: 10.1021/ct900587b.
31. Aier I, Varadwaj PK, Raj U. Structural insights into conformational stability of both wild-type and mutant EZH2 receptor. Sci Rep. 2016;6:34984. doi: 10.1038/srep34984.
32. Deniz U, Ozkirimli E, Ulgen KO. A systematic methodology for large scale compound screening: a case study on the discovery of novel S1PL inhibitors. J Mol Graph Model. 2016;63:110-24. doi: 10.1016/j.jmgm.2015.11.004.
33. Behera SK, Mahapatra N, Tripathy CS, Pati S. Drug repurposing for identification of potential inhibitors against SARS-CoV-2 spike receptor-binding domain: an in silico approach. Indian J Med Res. 2021;153(1 & 2):132-43. doi: 10.4103/ijmr.IJMR_1132_20.
34. Al-Nahain A, Jahan R, Rahmatullah M. *Zingiber officinale*: a potential plant against rheumatoid arthritis. Arthritis. 2014;2014:159089. doi: 10.1155/2014/159089.
35. Prasanth DS, Panda SP, Rao AL, Chakravarti G, Teja N, Vani VB, et al. In-silico strategies of some selected phytoconstituents from *Zingiber officinale* as SARS CoV-2 main protease (COVID-19) inhibitors. Indian J Pharm Educ Res. 2020;54(3s):s552-9. doi: 10.5530/ijper.54.3s.154.
36. Kumar S, Saini V, Maurya IK, Sindhu J, Kumari M, Kataria R, et al. Design, synthesis, DFT, docking studies and ADME prediction of some new coumarinyl linked pyrazolylthiazoles: potential standalone or adjuvant antimicrobial agents. PLoS One. 2018;13(4):e0196016. doi: 10.1371/journal.pone.0196016.
37. Ma CX, Ma XN, Guan CH, Li YD, Mauricio D, Fu SB. Cardiovascular disease in type 2 diabetes mellitus: progress toward personalized management. Cardiovasc Diabetol. 2022;21(1):74. doi: 10.1186/s12933-022-01516-6.
38. Peters KE, Davis WA, Beilby J, Hung J, Bruce DG, Davis TM. The relationship between circulating adiponectin, ADIPOQ variants and incident cardiovascular disease in type 2 diabetes: the Fremantle Diabetes Study. Diabetes Res Clin Pract. 2018;143:62-70. doi: 10.1016/j.diabres.2018.06.005.
39. Gupta C, Bubber P, Fahim M, Saidullah B, Omanwar S. Adiponectin in onset and progression of T2DM with cardiac dysfunction in rats. Hum Exp Toxicol. 2020;39(11):1463-74. doi: 10.1177/0960327120927446.
40. Ahn EK, Oh JS. Inhibitory effect of galanolactone isolated from *Zingiber officinale* roscoe extract on adipogenesis in 3T3-L1 cells. J Korean Soc Appl Biol Chem. 2012;55(1):63-8. doi: 10.1007/s13765-012-0011-6.